Mechanism and Machine Theory 116 (2017) 513–528

Contents lists available at ScienceDirect

Mechanism and Machine Theory

journal homepage: www.elsevier.com/locate/mechmachtheory

Research paper

Nonlinear load-deflection and stiffness characteristics of coned springs in four primary configurations

Nicholas P. Mastricola, Rajendra Singh*

Acoustics and Dynamics Laboratory and Smart Vehicles Concepts Center, Department of Mechanical and Aerospace Engineering, The Ohio State University, Columbus, OH 43210, USA

ARTICLE INFO

Article history:
Received 28 February 2017
Revised 5 June 2017
Accepted 6 June 2017

Keywords:
experimental methods
preload device
continuous nonlinearity
continuous nonlinearity
stiffness characterization
dry friction

ABSTRACT

Even though coned disk springs have been used as preload or isolation elements in mechanical design for over a century, prior research has used several simplifying assumptions in determining their static load-deflection relationships and their stiffness properties have been largely ignored. Accordingly, the entire displacement range is considered in this article, from fully unloaded height to flat height under quasi-static loading conditions. Friction is accounted for at the face-to-face disk spring contacts and at the disk spring edge-to-surface contacts, but is ignored in edge-to-edge contacts. New experimental results for a single coned disk element, the primary parallel stack configuration, and two primary series stack configurations are presented. Measured load-deflection characteristics are analyzed in the context of newly defined nine distinct regimes that are motivated by the physics. Hysteresis curves are also examined and compared with a refined load-deflection relation with interfacial and edge friction coefficients. Finally, a continuously nonlinear stiffness expression is analytically derived, which matches well with measurements but only over a limited range of displacements.

1. Introduction

Coned disk springs (as shown Fig. 1a), a subset of the diaphragm spring family, have been in use in machine design (such as preload elements) for over a century. Since they are highly customizable at an element level as attested to by a myriad of diaphragm springs produced [1–5], the stackable nature of disk springs allows for easy modification of the gross stiffness and damping parameters of a stack. The inherent adaptability of the disk spring's stiffness is especially unique because it can be made positive, zero, or negative [3,5–7]. The nonlinear stiffness exhibited by quasi-zero stiffness mechanisms has been conceptually found to be advantageous for several vibration isolation studies [8–13] though the disk spring is not explicitly mentioned. The literature focusing on disk springs is very sparse and primarily limited to static analyses presented from a design viewpoint [4,6–7,14–19]. In particular, the seminal paper of Almen and Laszlo [6] established the disk spring load-deflection relationship which remains as the theoretical groundwork for most subsequent disk spring research. Almen and Laszlo [6], heavily influenced by a simplified problem proposed by Timoshenko [14], made the following key assumptions: (i) the disk spring cross-section is small; (ii) the disk spring cross-section remains constant during the deformation process, but merely rotates about a neutral point; and (iii) the loads are distributed evenly around the disk spring in an an-

* Corresponding author.
E-mail address: singh.3@osu.edu (R. Singh).

http://dx.doi.org/10.1016/j.mechmachtheory.2017.06.006
0094-114X/

Nomenclature

a	Mid-surface outer radius
b	Mid-surface inner radius
c	Neutral circle radius
E	Young's modulus
h	Cone height
k	Analytically determined stiffness
k	Piecewise nonlinear stiffness
M	Moment
n	Number of springs
P	Spring force resultant
x	Displacement
α	Radii ratio (a/b)
β	Cone base angle
δ	Axial spring deflection
γ	End point of stiffness regime
ε	Strain
η	Cone height to thickness ratio (h/t)
θ	General angle
κ	Slope of linear stiffness model section
μ	Static coefficient of friction
ν	Poisson's ratio
σ	Stress
τ	Shell thickness
Υ	Comparison model
φ	Relative rotational displace of disk spring cross-section
Φ	Displacement regime
ψ	Planer angle of disk spring

Subscripts

a	Outer edge
b	Inner edge
D	Disk spring
e	Edge
E	Experiment
F	Friction (includes friction)
Flat	Related to the disk spring or stack in the flat position
H	Linear helical spring
$L1$	Literature – Ref. [6]
$L2$	Literature – Ref. [19]
$L3$	Literature – Ref. [26]
n	Fundamental
p	Relating to the parallel disk spring contact
P	Manifests due to spring force
r	Radial component
$R1$	Reaction due to radial displacement
$R2$	Reaction due to change in curvature
t	Tangential component
ϕ	Face or interfacial

nularly symmetric fashion. Several aspects of the Almen-Laszlo relationship were re-examined by researchers [7,15–16] who specifically focused on practical design methodology.

Curti *et al.* [17–20] noted that Almen and Laszlo correctly assumed that radial stress σ_r is negligible ($\sigma_r = 0$); nevertheless, radial strain ε_r was considered to be negligible ($\varepsilon_r = 0$) throughout the Almen–Laszlo derivation. Curti and Orlando [17–18] derived an alternate analytical load-deflection relationship by treating the coned disk spring as a flat plate of small thickness with a hole and coupling the radial and tangential stresses. Their derivation [17–18] resulted in a load-deflection expression which differed from the Almen–Laszlo [6] relationship by a multiplicative factor of $1 - \nu^2$, where ν is Poisson's ratio. Subsequently, Curti *et al.* [19] achieved the same result through a greatly simplified, but more illustrative, means of correctly applying within a framework similar to that of Almen and Laszlo [6].

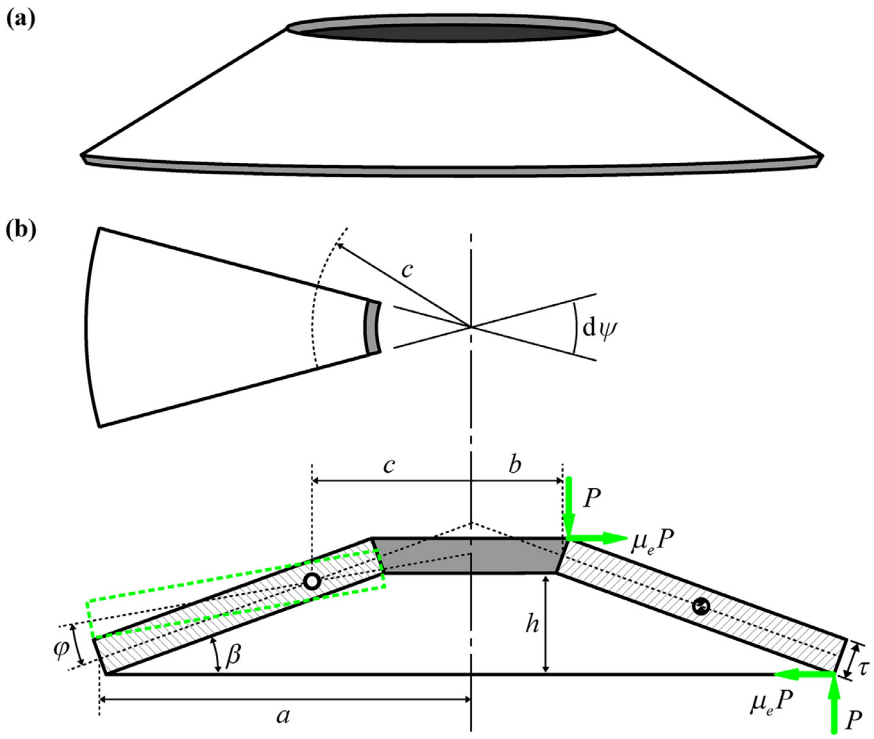

Fig. 1. Coned disk spring element: (a) Square-edged element (configuration Υ_1); (b) overhead and cross-section view of a coned disk spring with standard geometric parameters and load points. Key: ⟶ force, ▬ ▬ deformed position of cross-section. Remaining symbols are defined in the text and in the *Nomenclature* section.

Additionally, only a limited number of experimental studies have been reported in the literature [2,6,17–26] in the context of validation and verification of analytical expressions; however, most measurements data sets were limited to the midrange displacements such that the initial loading phase and ending stopper phase could be avoided. Also, assumptions have been made in literature as to the behavior of the disk spring as a singular element or as an entity within a disk spring stack. Wahl [7], to the best of the authors' knowledge, published the first measurement, which included the aforementioned terminal effects and was accompanied by heuristic comparison to the Almen–Laszlo load-deflection relationship [6]. Curti *et al.* [21] made a similar comparison between their experiment and analytical expressions suggested by Almen and Laszlo [6] as well as Curti *et al.* [18–19]. Other experimental studies [22–26, 28] have largely focused on characterizing the nature of friction at the disk spring boundaries and the determination of its effect.

The influence of disk springs on the dynamics of physical systems has been studied to a much lesser extent. For example, Bühl [27] characterized the general loss properties of a disk spring stack by determining a damping coefficient using the logarithmic decrement method for a range of preloads. Ozaki *et al.* [28] performed quasi-static characterization of disk spring stacks for the purpose of constructing a computational (finite element) model of the disk spring where both dry friction and viscous damping were lumped into a general energy dissipation term. Numerical studies, using the proposed finite element method model, were conducted on a simple mass-spring oscillator and transmissibility curves that exhibited stiffening behavior were predicted [28–29].

To overcome certain voids in the literature, the chief goal of this article is to experimentally and analytically characterize the nonlinear load-deflection relations and to clarify the stiffness regimes and their transition points. The scope of this paper is limited to commercially available square-edged disk springs which are stackable in primary configurations as displayed in Fig. 2 and listed in Table 1. The entire displacement range is considered, from fully unloaded height to flat height, and friction will be accounted for at the face-to-face disk spring contacts (in parallel stack configurations) and at the disk spring edge-to-surface contacts, but will be ignored in edge-to-edge contacts.

2. Problem formulation

The focus of this article is confined to the examination of single disk springs and stacks assembled from two disk springs in the primary stack configurations as shown in Figs. 2a–c and named in Table 1. The specific objectives are: first, measure the full-range load-deflection characteristic of a disk spring and primary stack configurations and analyze them in terms of their naturally arising transition points and hysteretic behavior; second, propose a refined disk spring load-deflection formulation with edge and interfacial friction and to compare predictions with measurements; and third, examine the stiffness

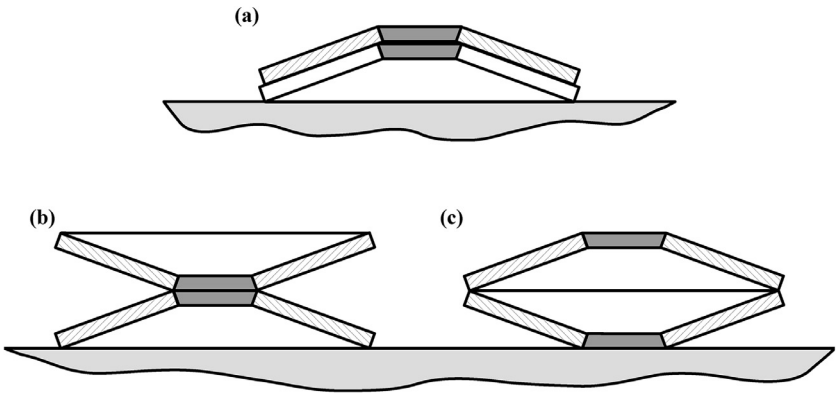

Fig. 2. Typical stack configurations using two coned disk elements: (a) parallel (configuration Υ_2); (b) inner series (configuration Υ_3); and (c) outer series (configuration Υ_4). Refer to Table 1 for a summary of the configurations analyzed in this article.

Table 1
Designations used for stack configurations of coned disk springs.[a]

Symbol	Stack configuration
Υ_1	Single disk spring (Fig. 1)
Υ_2	Parallel stack (Fig. 2a)
Υ_3	Inside edge series stack (Fig. 2b)
Υ_4	Outside edge series stack (Fig. 2c)

[a] The R8 ball bearing disk springs are used throughout this article (purchased from McMaster-Carr on www.mcmaster.com).

nonlinearity and propose distinct regimes. Full-range load-deflection characteristics of the disk spring and primary stack configurations (from unloaded height to flat height) are experimentally acquired, under quasi-static loading conditions, using the apparatus shown in Fig. 3. The experimental results will be analyzed from a load-deflection perspective (in terms of transition point location and hysteresis), and in terms of their stiffness characteristics. The stiffness results presented herein will be compared to the prior literature, including a few studies which use similar nonlinear stiffness characteristics without the use of disk springs.

The following classical assumptions [6] for analyzing disk springs will be applied throughout the presented experimental and analytical work such that the analytical and experimental methods used can draw upon, and be compared with, prior studies on equal footing — (i) the disk spring cross-section is small; (ii) the disk spring cross-section rotates about a neutral point and does not deform during the loading or unloading process; and (iii) forces are evenly distributed about the disk spring edges in an annularly symmetric fashion. Additionally, friction between disk spring edges and the platen faces (Fig. 3) and at interfacial contacts between disk spring faces — configuration Υ_2 (Fig. 2a) — will be considered throughout the analysis. However, the friction at disk spring edge-to-edge contacts is considered negligible.

3. Analytical load-deflection relationships of primary disk spring stacks

The Almen–Laszlo load-deflection relationship [6] for a single disk spring is formulated through the moment equilibrium condition (with reference to Fig. 1b) as

$$\mathrm{d}M_P = \mathrm{d}M_{R1} + \mathrm{d}M_{R2}, \tag{1}$$

where differential moment $\mathrm{d}M_P$, arises from the reaction force P, $\mathrm{d}M_{R1}$ is the radial displacement reaction moment, and $\mathrm{d}M_{R2}$ is the reaction moment which manifests from the change in curvature. In Eq. (2), $\mathrm{d}M_P$ is expressed in terms of disk spring thickness τ; cone base angel β; relative rotational displacement φ; planer angle ψ; and the inner and outer mid-surface radii a and b, respectively. Note that the simplifying approximations $\cos(\beta-\varphi)\approx 1$ and $\sin(\beta-\varphi)\approx\tan(\beta-\varphi)\approx\beta-\varphi$ are applied since both β and φ are small.

$$\mathrm{d}M_P = \frac{P}{2\pi}[(a-b)-\tau\sin(\beta-\varphi)]\cdot\mathrm{d}\psi \approx \frac{P}{2\pi}(a-b)\cdot\mathrm{d}\psi. \tag{2}$$

Next, $\mathrm{d}M_{R1}$ and $\mathrm{d}M_{R2}$ are expressed in the same manner as $\mathrm{d}M_P$ with the addition of Young's modulus E and the radii ratio α, where $\alpha = a/b$.

$$\mathrm{d}M_{R1} = E\tau\varphi(\beta-\varphi)\left(\beta-\frac{\varphi}{2}\right)\left(\frac{a^2-b^2}{2}-\frac{(a-b)^2}{\ln\alpha}\right)\cdot\mathrm{d}\psi \tag{3}$$

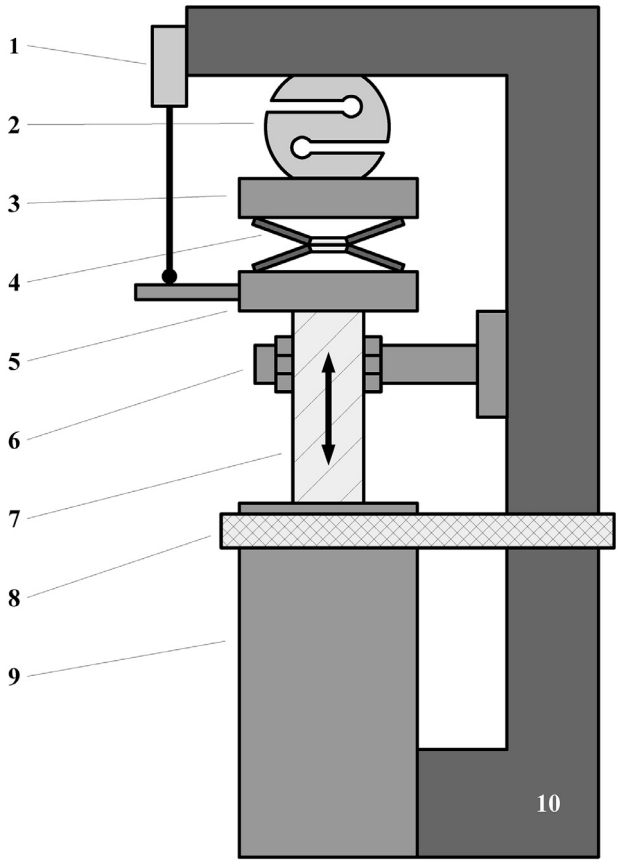

Fig. 3. Quasi-static experiment proposed to measure the load-displacement curve of coned disk springs. Key of components: (1) high resolution LVDT, (2) force transducer, (3) upper platen, (4) disk spring or stack, (5) lower platen, (6) centering support assembly, (7) power screw, (8) tensioning support band, (9) power screw body, and (10) rigid outer support, where ◄► is the line of action of the power screw.

$$dM_{R2} = \frac{E\tau^3\varphi}{12}\ln\alpha \cdot d\psi \tag{4}$$

Substitution of Eqs. (2)–(4) into Eq. (1), with the axial spring deflection, yields the well-known Almen–Laszlo relationship [6]

$$P_{L1}(\delta) = \frac{E\delta\pi}{(1-\nu^2)a^2}\left(\frac{\alpha}{\alpha-1}\right)^2\left[\tau(h-\delta)\left(h-\frac{\delta}{2}\right)\left(\frac{\alpha+1}{\alpha-1}-\frac{2}{\ln\alpha}\right)+\frac{\tau^3\ln\alpha}{6}\right]. \tag{5}$$

Using two separate methods, the Almen–Laszlo expression was simplified by Curti *et al.* [17–19] to

$$P_{L2}(\delta) = \frac{E\delta\pi}{a^2}\left(\frac{\alpha}{\alpha-1}\right)^2\left[(h-\delta)\left(h-\frac{\delta}{2}\right)\left(\frac{\alpha+1}{\alpha-1}-\frac{2}{\ln\alpha}\right)\tau+\frac{\tau^3\ln\alpha}{6}\right]. \tag{6}$$

Curti *et al.* [26] modified Eq. (6) to include the edge friction using an analogous method to that used by Almen and Laszlo [6], which takes the form

$$P_{L3}(\delta) = \frac{P_{L2}(\delta)}{1 \mp \mu_e\frac{(h-\delta+\tau)}{a-b}}, \tag{7}$$

where μ_e is the coefficient of friction at the disk spring edge. Niepage [24] added a term for edge friction and disk spring face-to-face friction, though this was accomplished by rather tedious algebraic means.

In this article, Eq. (7) is modified to include face-to-face friction by a more compact method which is a closer analog to the methods used in prior formulations [6, 17–19, 26]. Hence, the friction between disk spring faces in the parallel configuration (Fig. 2a) and the disk spring edge to surface friction — in the cases of the single disk spring (Fig. 1a) or series stacks (Figs. 2b–c) — are accounted for by formulating appropriate differential moment terms, which can be added to Eq. (1). Thus,

$$dM_P = dM_{R1} + dM_{R2} + dM_{\phi F} + dM_{eF}, \tag{8}$$

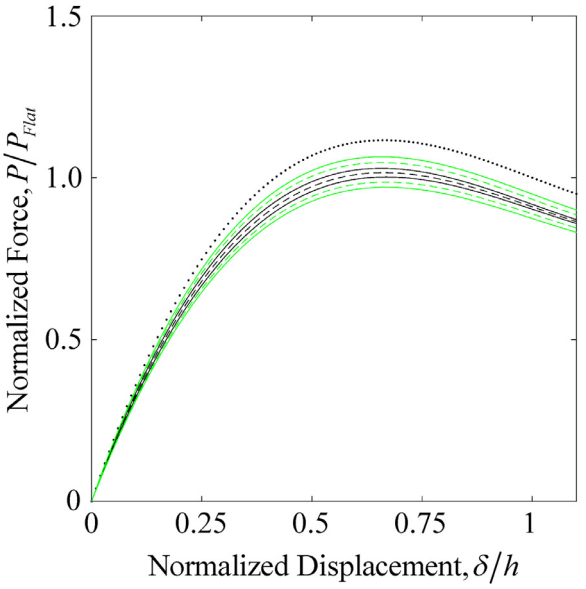

Fig. 4. Comparison of prior and proposed analytical formulations. Key: ●●●●● $P_{L1}(\delta)$, ▬ ▬ ▬ $P_{L2}(\delta)$, ▬▬▬ $P_{L3}(\delta)$ with $\mu_e = 0.1$ (equivalent to $P_F(\delta)$ with $\mu_e = 0.1$ and $\mu_\phi = 0$), ▬ ▬ ▬ $P_F(\delta)$ with $\mu_e = 0.1$ and $\mu_\phi = 0.2$, ▬▬▬ $P_F(\delta)$ with $\mu_e = 0.1$ and $\mu_\phi = 0.4$.

where $dM_{\phi F}$ is the differential moment due to the face-to-face disk spring friction and dM_{eF} is the differential moment due to the friction between the disk spring edge and its supporting surface. Both $dM_{\phi F}$ and dM_{eF} may be written in the form of the other differential moments with the addition of the coefficients of friction between the disk spring faces and the disk spring edge to surface contact — μ_ϕ and μ_e, respectively — and the number of parallel contacts (n_p) between disk springs in a stack as

$$dM_{\phi F} = \pm\mu_\phi \frac{P\cos(\beta-\varphi)n_p\frac{\tau}{2}}{2\pi}\cdot d\psi \approx \pm\mu_\phi \frac{Pn_p\frac{\tau}{2}}{2\pi}\cdot d\psi \tag{9}$$

and

$$\begin{aligned} dM_{eF} &= \pm\frac{\mu_e P}{2\pi}[(a-b)\tan(\beta-\varphi)+\tau\cos(\beta-\varphi)]\cdot d\psi \\ &\approx \pm\frac{\mu_e P}{2\pi}[(a-b)(\beta-\varphi)+\tau]\cdot d\psi. \end{aligned} \tag{10}$$

The more general load-displacement relationship is then found, as shown in Eq. (11), by applying the small angle approximations, changing the variables β and φ to their linear counterparts h and δ, and substitution into Eqs. (2)–(4) and Eqs. (9)–(10) into Eq. (8).

$$P_F(\delta) = \frac{P_{L2}(\delta)}{1 \mp \left[\frac{\mu_e(h-\delta+\tau)+\mu_\phi\frac{\tau}{2}n_p}{a-b}\right]} \tag{11}$$

As should be expected, Eq. (11) does not explicitly depend on the number of disk springs in series since the disk spring edge-to-edge contacts are being considered to be essentially frictionless rolling contacts and there are only ever two disk spring edge-to-surface contacts at the terminal ends of the stack. By setting $\mu_\phi = 0$ or $n_p = 0$, Eq. (11) reduces to $P_{L3}(\delta)$ — the result of Curti et al. [26] as shown in Eq. (7). Further, Eq. (11) is shown to reduce to $P_{L2}(\delta)$, shown as derived by Curti et al. [19] in Eq. (6), by setting $\mu_e = \mu_\phi = 0$; therefore, Eq. (11) is a further generalization of both aforementioned formulations. Likewise, the relationships between Eqs. (5)–(6) and Eq. (11) are shown in Fig. 4 with assumed values of μ_e and μ_ϕ. An addition of the interfacial friction term does indeed increase the amount of hysteresis, and does so successively with increasing μ_ϕ. As one should expect, Fig. 4 also shows that Eqs. (5)–(6) are incapable of accurately describing the parallel contacts between disk springs. Eq. (11) will, therefore, be used to assess the role of interfacial friction in hysteresis of disk springs stacked in parallel. Measurements will be used to quantify the values of both μ_e and μ_ϕ.

4. Experimental method

Disk springs are low profile and small footprint devices that, by their nature, are able to produce extreme forces at relatively low displacements. While these unique qualities have been leveraged considerably in their use as preload devices [1, 5–7] and show great promise in use as vibration isolation elements [8–13], the orders of magnitude scale difference

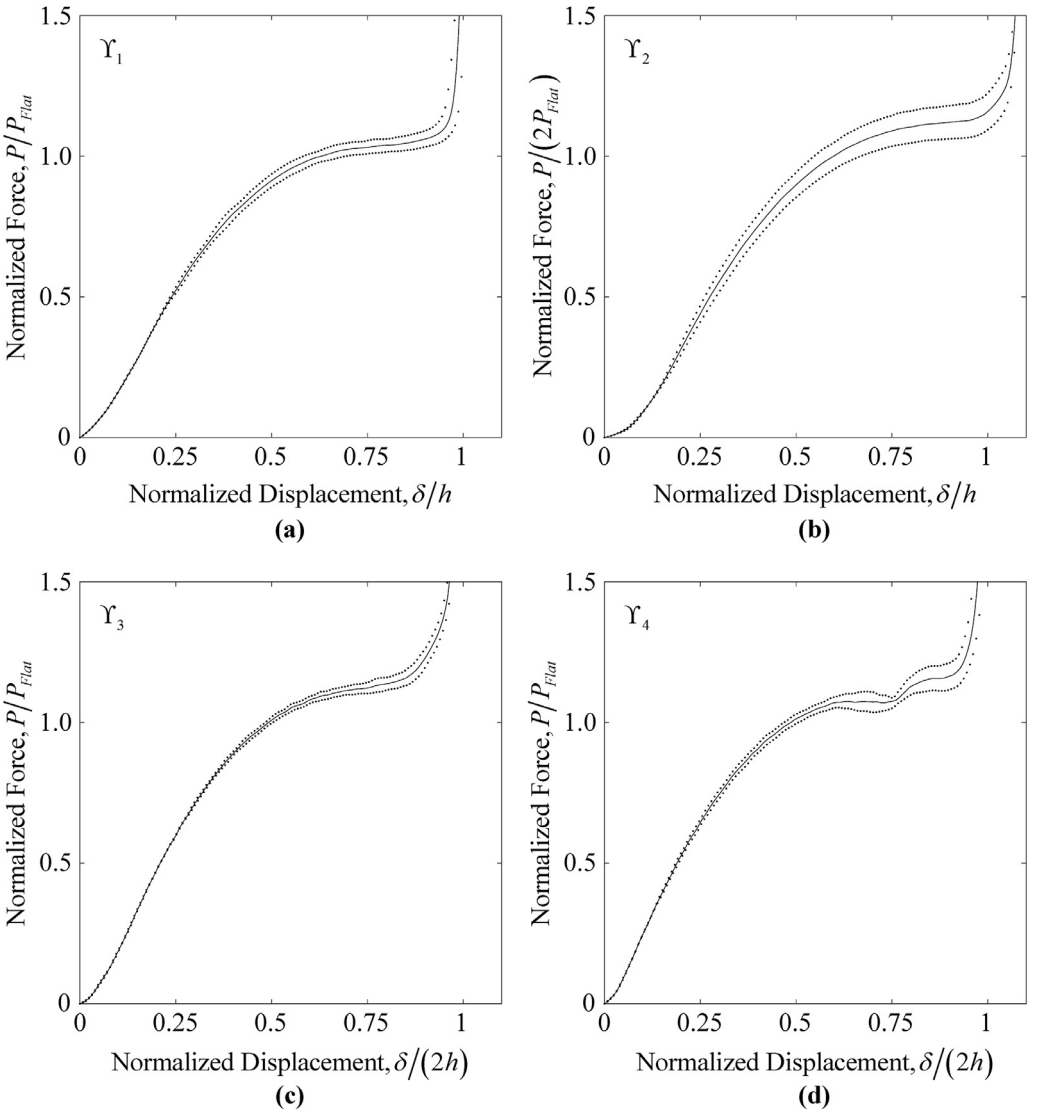

Fig. 5. Measured load-deflection (normalized) characteristics for four configurations of Table 1 and Figs. 1 and 2:(a) Υ_1, (b) Υ_2, (c) Υ_3, and (d) Υ_4. Key: ●●●●● measured loading and unloading characteristics, ▬▬ computed median characteristic from measurements.

between input displacement and output force make them exceedingly difficult to experimentally evaluate. Likewise, the physical scale of disk springs also creates unique challenges when attempting to maintain alignment of the disk spring primary stack configurations Υ_2,Υ_3, and Υ_4 (Figs. 2a–c) when they are under a load without an external means of alignment. The final design of the experiment, shown in Fig. 3, as well as the experimental methods shown herein are similar to those recently described by Mastricola et al. [30]. As shown previously, the displacement (δ) of the lower platen is measured by a ground-fixed high resolution linear variable displacement transformer (LVDT). There are no special requirements of the force sensor other then it is able to hold tolerance over the large range of spring force (P) produced by the disk spring or stack under test. The functionality of the experiment is verified by the same method outlined in Mastricola et al. [30].

5. Measured full-range load-deflection characteristics and comparison with theory

The measurements obtained from the single disk spring configuration (Υ_1) using the quasi-static test apparatus (Fig. 3), are shown in Fig. 5a. These are normalized by the theoretically predicted flattening load P_{Flat}, as derived for a single disk spring [3]

$$P_{Flat} = \frac{\pi E h \tau^3}{a^2\left(1-\nu^2\right)}\left(\frac{\alpha+1}{\alpha-1}-\frac{2}{\ln\alpha}\right)\left(\frac{\alpha}{\alpha-1}\right)^2. \tag{12}$$

Table 2
Summary of distinct load-displacement regimes as displayed in Fig. 7 and normalized end transition points for four configurations.

Regime	Description (using measurements)	Regime end transition points (normalized), δ/h			
		Υ_1	Υ_2	Υ_3	Υ_4
Φ_1	Initial engagement	0.0505	0.0617	0.0255	0.0179
Φ_2	Transition to analytical behavior	0.1515	0.1724	0.0805	0.0419
Φ_3	Analytical behavior	0.6402	0.4896	0.2612	0.2431
Φ_4	Transition into primary plateau	0.7633	0.8409	0.6618	0.5979
Φ_5	Primary plateau	0.8431	0.9686	0.8503	0.7593
Φ_6	Transition into secondary plateau	–	–	–	0.8470
Φ_7	Secondary plateau	–	–	–	0.8947
Φ_8	Transition into stopper	0.9592	1.037	0.9387	0.9367
Φ_9	Stopper (end point at $P/P_{Flat} = 3$)	1.023	1.068	0.9822	1.006

As one should expect, disk springs in parallel (Fig. 2a) will add just as two linear springs with a negligible increase in the amount of deflection required. As such, the measured load-displacement characteristics of configuration Υ_2 (Fig. 5b) are normalized by $2P_{Flat}$. Due to the nature of disk springs, series stacks (Figs. 2b–c) will have the same flattening load as a single disk spring; however, they will require twice the deflection. Thus, the load-deflection measurements obtained from configurations Υ_3 and Υ_4 are also normalized by P_{Flat} and then displayed in Figs. 5c and 5d, respectively. Further, the operating deflections of Υ_1 and Υ_2 (Figs. 5a and 5b, respectively) are normalized by h such that $\delta/h = 1$. From the predicating geometric restriction, the domains of configurations Υ_3 and Υ_4 (Figs. 5c and 5d, respectively) are normalized by $2h$. A consistent method is determined in order to isolate the load-deflection characteristics from extraneous data by using clear landmarks in the measurements that are indicative of the disk spring, or stack, making first contact with the force sensor and at the point of total flatness. The load-deflection characteristics appear to be comprised of several continuous nonlinear regimes (leading up to the point of impending flatness) and one discontinuous nonlinear regime (the so-called stopper effect witnessed at the point of impending flatness) for the characteristics obtained from configurations Υ_1, Υ_2, andΥ_3 (Figs. 5a–c). However, there are marked changes in the load-deflection characteristic of configuration Υ_4 (Fig. 5d), in which several additional regimes are observed. While it could be argued that the manifestation of extra regimes is a mere aberration that could easily be disregarded, they do arise in several different combinations of disk springs over multiple tests. The load-deflection characteristics shown in Fig. 5 emerge as the clear typical characteristics for their respective configurations through the testing of several different disk spring pairs. However, throughout the measurements, it has been found that a small number of disk spring pairs produce atypical curves (shown in Fig. 6). The inside series and the more unusual outside series load-deflection characteristics, Figs. 6b and 6d, respectively, show two crossings of the unloading and loading curves. This shows, for the majority of the displacement range, that these particular pairs produce higher forces during the unloading phase rather than the loading phase when in configurations Υ_3 and Υ_4.

Albeit possible by observation to make the assertion that there are several continuous nonlinear regimes, the majority of their transition points are, at best, indistinct. Initially, two numerical derivatives were computed with the idea that their zero-crossings or inflection points would be at or near the transition points; however, this was quickly discarded because, even after smoothing of the resulting derivatives, the fidelity of this method did not hold from measurement to measurement. However, since the majority of the load-deflection characteristics have smooth transitions between nonlinear regimes, this method was also rejected. In essence, both of the attempted methods for locating the regime transition points failed due to the fact that there are few distinct landmarks in the load-deflection characteristic that can be utilized for a consistent determination of the regime transition; therefore, it is imperative to impose a quasi-fixed reference to which the measured data could be compared. As a reference, $P_{L2}(\delta)$ is chosen for use with the median load-deflection characteristic calculated from the measurement (Fig. 5). For the task at hand, a distinct regime is considered a section of the measured characteristic wherever it deviates in a significant manner from the analytical curve. The segments that deviate from the analytical curve are treated in a quasi-linear fashion; thus, tangent lines are constructed on the measured characteristic in order to determine the transition points between two quasi-linear continuous (nonlinear) regimes. In essence, this creates a piecewise nonlinear function since all aspects of the measurements cannot be captured in a single expression; however, the resultant is still smooth and continuous in nature.

Applying the previously mentioned method to the median load-deflection characteristic of configuration Υ_1 (Fig. 5a), six load-deflection regimes are observed, as clearly depicted in Fig. 7a. Key results are summarized in Table 2. Regimes (or transitions) Φ_1 to Φ_3, Φ_5, and Φ_8 to Φ_9 (reference Table 2) are called the principal regimes since they are found in all configurations. Note that $P_{L2}(\delta)$ is offset during the initial regimes Φ_1 and Φ_2. This is not all together unexpected due to the classical Almen–Laszlo [6] assumption that the loads are evenly distributed about the edges of the disk spring which implies that at the beginning of the curve the disk spring has sufficient preload to bring the edges of the disk spring into even and complete contact. Conversely, these initial regimes, although not reported as such, are consistent with limited experimental data that has been reported in the prior literature [7, 19, 21, 23, 27]. In particular, Wahl [7], only showing data from a parallel stack, made the assertion that the initial regimes were caused by the flattening of irregularities between

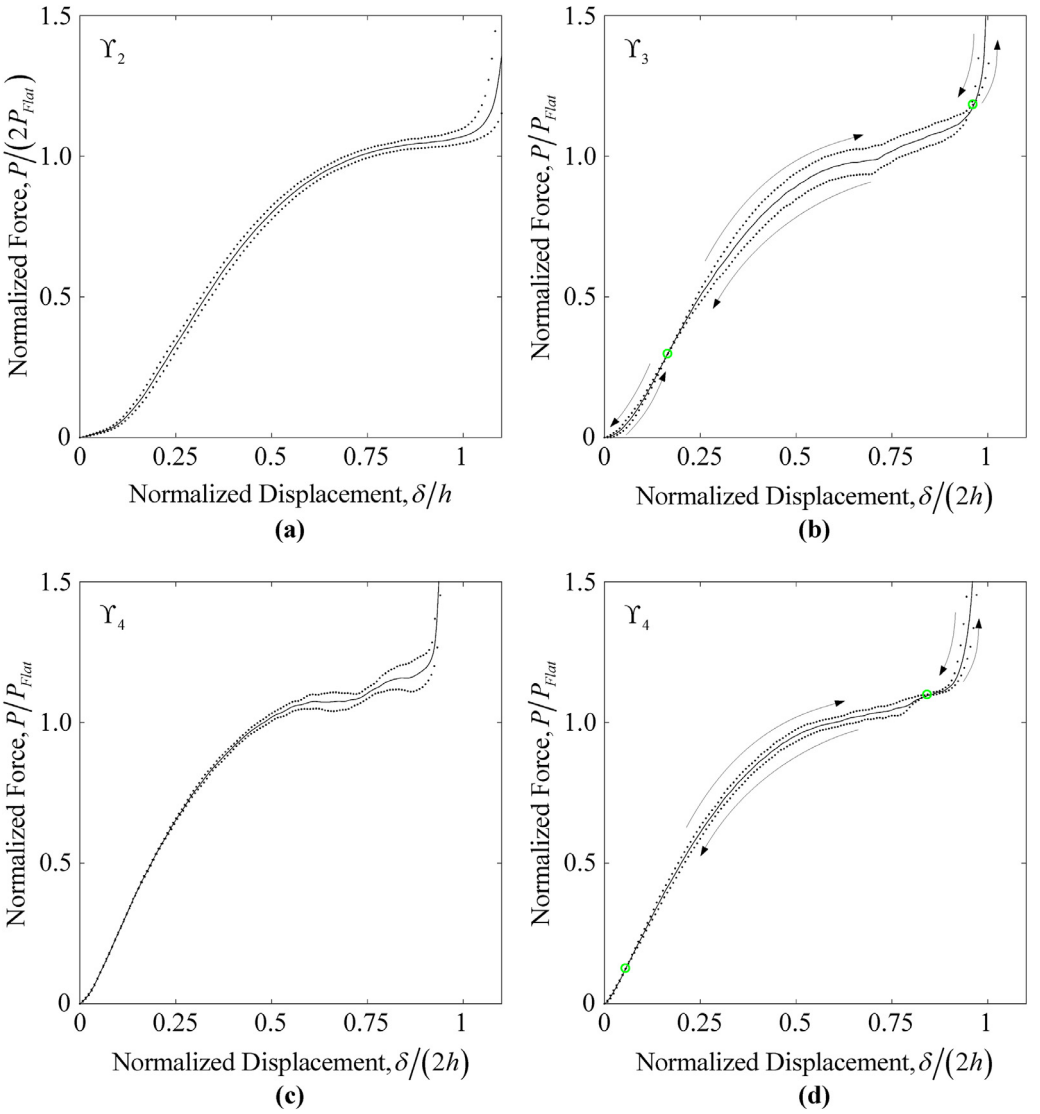

Fig. 6. Variations in load-deflection characteristics due to disk spring pairings: (a) Υ_2, (b) Υ_3, (c) Υ_4 – variation of standard form, (d) Υ_4 – variation produced by a poorly matched pair. Key: ●●●●● measured loading and unloading characteristics, ▬▬ computed median characteristic from measurements, ○ loading-unloading cross point.

disk springs; however, as shown in Fig. 7, this behavior is exhibited by all configurations under consideration. Hence, it is reasonable to hypothesize that regimes Φ_1 and Φ_2 arise from slight asymmetries or irregularities of the disk spring's load bearing edges in configurations other than Υ_2. Regime Φ_3, as shown in Fig. 7a, is reasonably approximated by the analytical curve; however, there is a strong divergence between theory and experiment when the load-defection characteristic plateaus (regime Φ_5). Likewise,Φ_8, and Φ_9 are not accounted for by the analytical expression because the assumption is made that the disk spring is not constrained in the vertical direction and would be allowed to travel such that $\varphi < 0$, which is seldom found in practical application due to the fixture considerations.

In the load-displacement measurements from configurations Υ_2 and Υ_3 (Fig. 7b and 7c, respectively), another transition regime (Φ_4) is observed going from Φ_3 to Φ_5. While the length of Φ_5 is relatively unchanged, there is a marked shortening of regime Φ_3, which may be attributed to yet undescribed interplay between the disk spring elements in the stack. The load defection characteristic from configurationΥ_4 (Fig. 7d), albeit seemingly more complicated due to the arising of three regimes in addition to the principal regimes, has an elegantly simple explanation. Due to the placement of regimes Φ_7 and Φ_8 it is possible to make the assertion that one spring in the pair is slightly more compliant than the other. This has the ramification that the weaker of the paired springs will have an increase in stiffness slightly before the other; hence, the stiffer spring in the pair will only continue to deflect once the softer spring can carry the appropriate load.

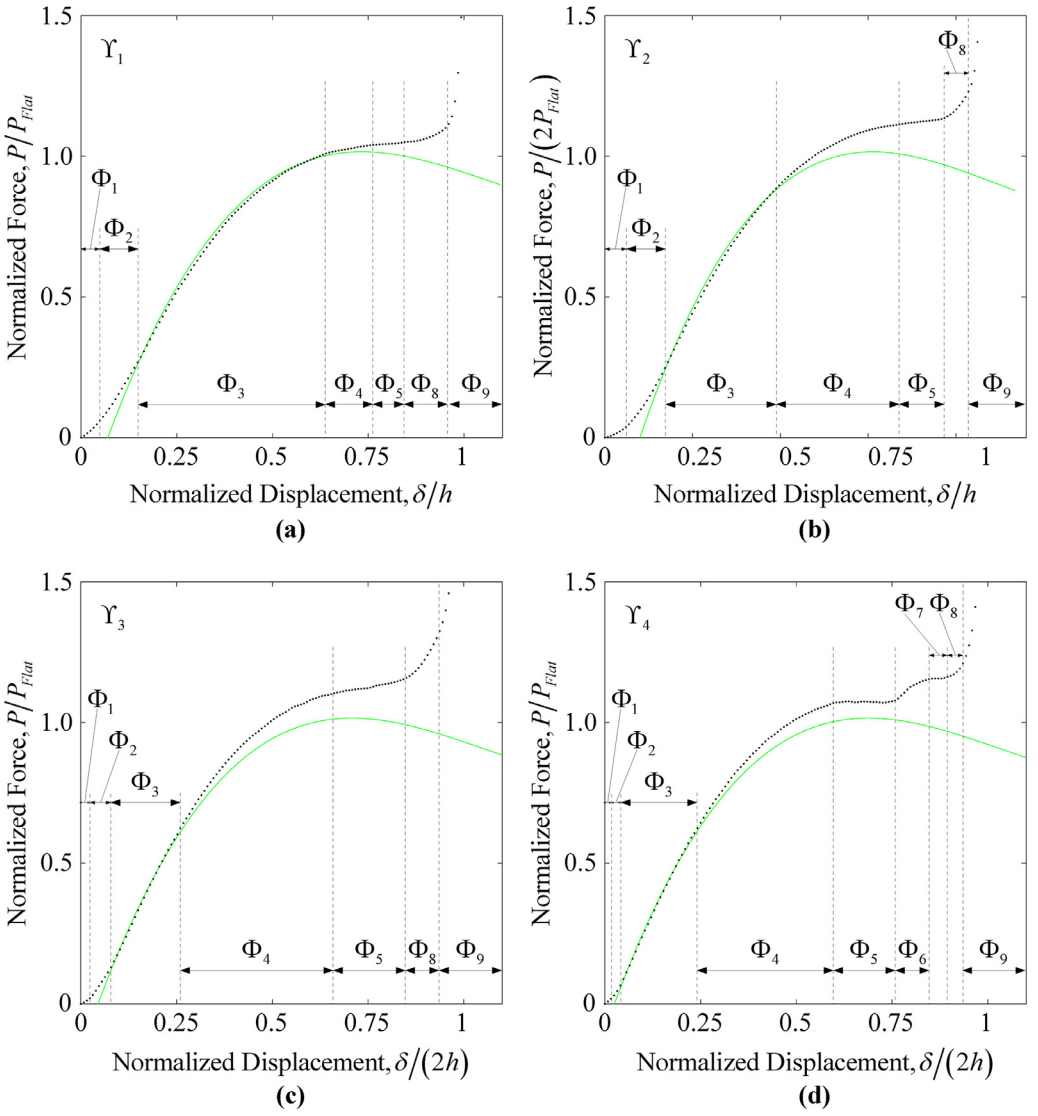

Fig. 7. Comparison of measured and analytical load-deflection characteristics and identification of multiple regimes (Φ) for four configurations: (a) Υ_1, (b) Υ_2, (c) Υ_3, and (d) Υ_4. Key: ●●●●● measured (computed median characteristic) from measurement, ▬ predicted using $P_{L2}(\delta)$ expression.

6. Hysteretic force measurements and comparison with theory

Eq. (11) is used to determine the theoretical hysteretic behavior that should be exhibited over displacement region Φ_3. From prior comparisons made in this article, it has been shown that the best agreement between theory and experiment is exhibited by configuration Υ_1. Therefore, it can be assumed that μ_e determined from this configuration may be applied to all of the configurations listed in Table 1 since only two disk spring edge-to-surface contacts are seen in any disk spring stack configuration. For configurationΥ_1, Eq. (11) is applicable by setting both n_p and μ_ϕ to zero, and thereby reducing Eq. (11) to $P_{L3}(\delta)$ — Eq. (7). The friction coefficient at the disk spring's edge, μ_e, may now be estimated by varying its value with comparison to the measured hysteresis loop of configuration Υ_1. Sufficient agreement in Φ_3 of Υ_1 is observed between theoretical and measured hysteresis forces at $\mu_e = 0.12$, which is consistent for a galvanized steel-steel contact. The result of tuning μ_e for the single disk spring configuration (shown in Fig. 8a) is consistent with agreement shown by Curti *et al.* [26] as should be expected. Likewise, as listed in Table 3, this value of μ_e is applied to all remaining configurations as shown in Fig. 8. Without any further parameter tuning, reasonable agreement is seen in regime Φ_3 for configurations Υ_3 and Υ_4. However, configurations Υ_1, Υ_3, and Υ_4 all exhibit a departure of theory from measurement in the transitional regime Φ_4; much longer transitional regimes are witnessed in both series configurations (Figs. 8c and 8d). Furthermore, after theory and measurement values diverge for configurations Υ_3, and Υ_4, the under-predicting trend is clearly seen from the remaining displacement regimes. To a much lesser extent, this trend is also seen in configuration Υ_1.

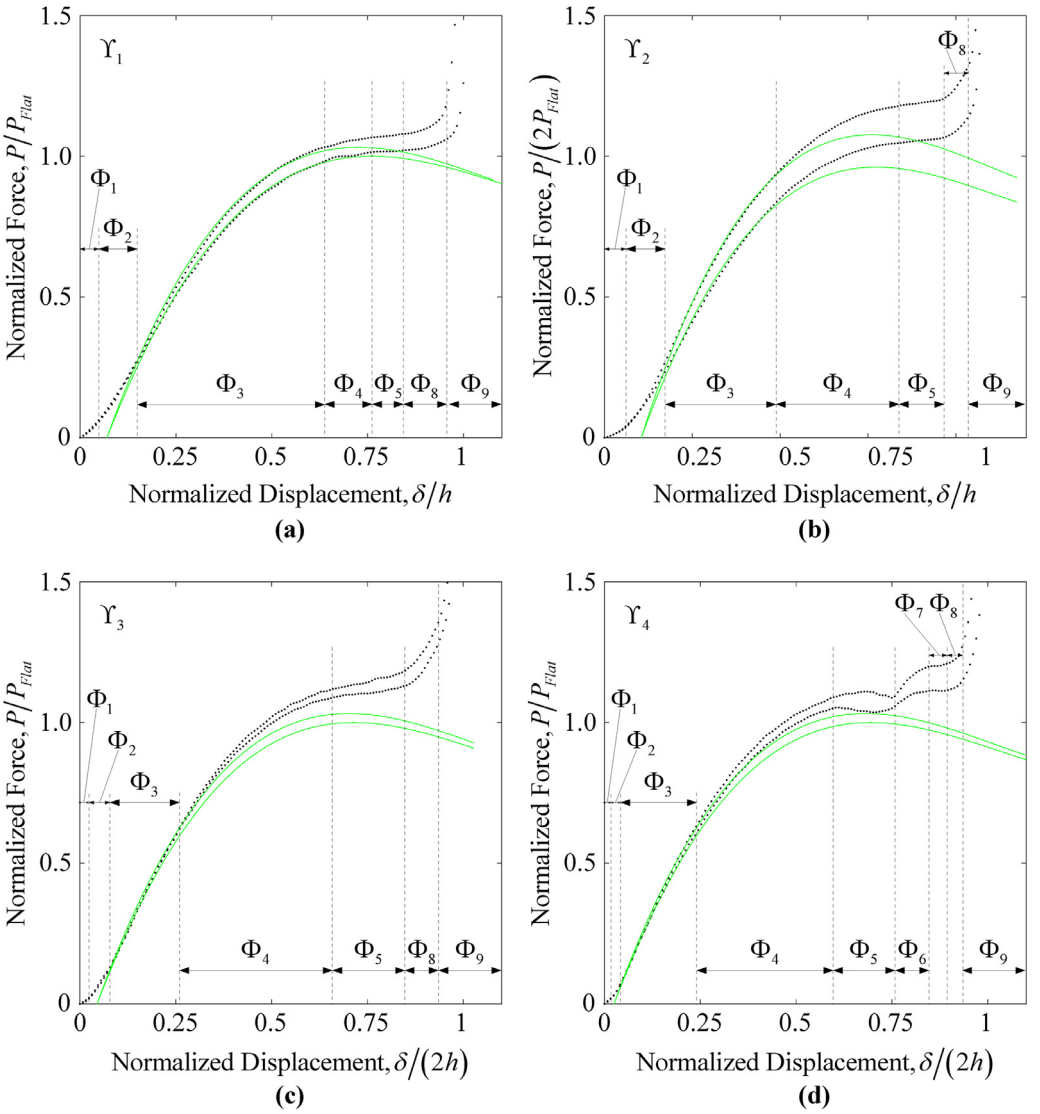

Fig. 8. Measured and predicted load-displacement characteristics for four configurations of Table 1 and Figs. 1 and 2: (a) Υ_1, (b) Υ_2, (c) Υ_3, and (d) Υ_4. Key: ●●●●● measurement, ▬ Eq. (11) prediction.

Table 3
Disk spring edge and interfacial surface friction coefficients, μ_e and μ_ϕ, respectively, estimated using Eq. (11), with reference to results of Fig. 7.

Coefficient of friction	Disk spring stack configuration			
	Υ_1	Υ_2	Υ_3	Υ_4
μ_e	0.12	0.12	0.12	0.12
μ_ϕ	–	0.49	–	–

Using a similar tuning method as used for the estimation of μ_e, μ_ϕ is found to be 0.49 (Table 3) using Eq. (11) with $n_p = 1$ for configuration Υ_2. The resulting value of μ_ϕ is consistent with published values for steel-steel contacts. Comparing the hysteresis curves of configurations Υ_1 and Υ_2 — Fig. 8a and b, respectively — a distinct increase in hysteresis is observed. Since the edge friction is assumed to be equal in all configurations, the approximate 74% increase in hysteresis loop width between configurations Υ_1 and Υ_2 can be reasonably attributed to the friction forces between the inner and outer surfaces of the disk spring. The point of comparison between was chosen to be the greatest normalized displacement in the analytical regime of configurationΥ_2. As with the other cases, a distinct divergence between theory and measurement is observed in

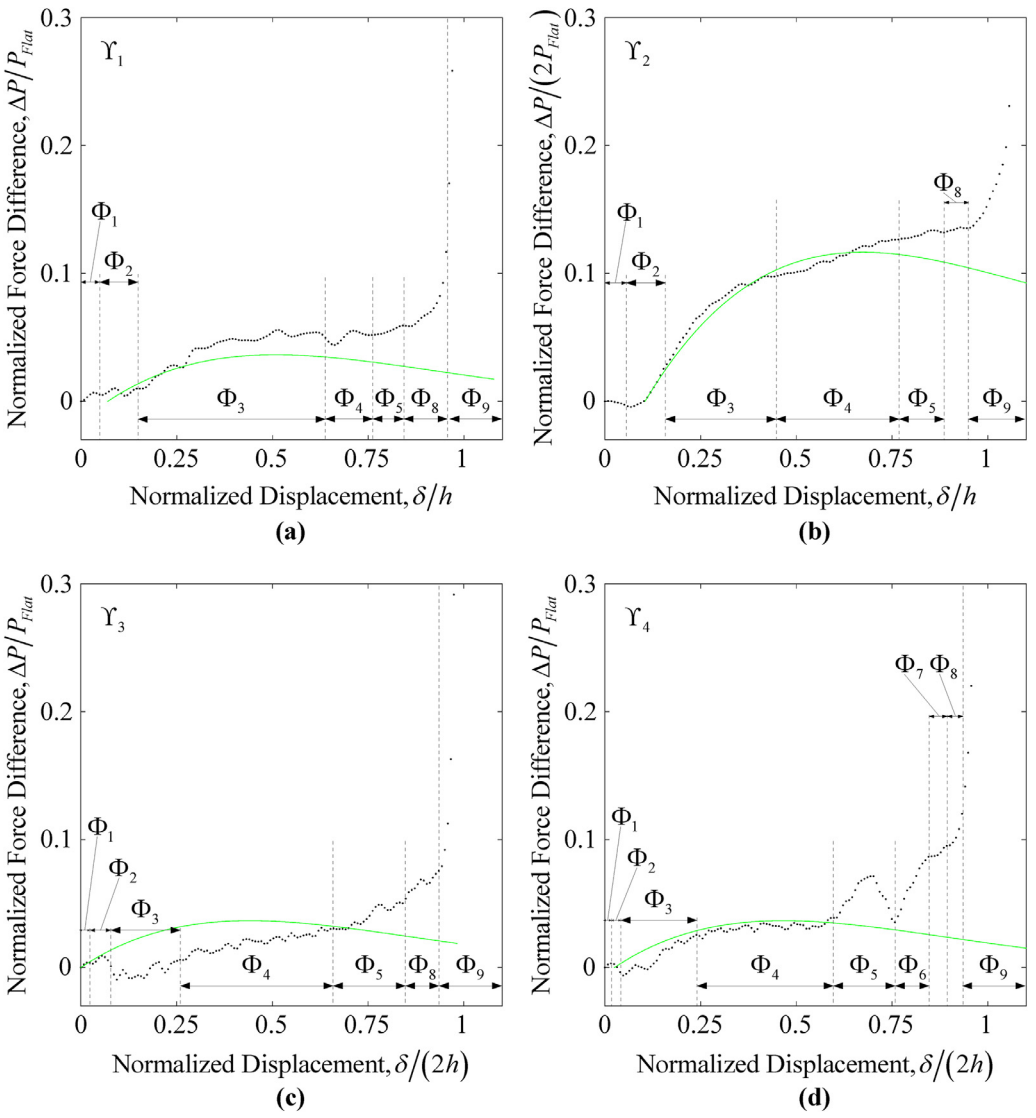

Fig. 9. Measured and predicted hysteresis characteristics for four configurations of Table 1 and Figs. 1 and 2:(a) Υ_1, (b) Υ_2, (c) Υ_3, and (d) Υ_4. Key: ●●●●● measurement, ▬ prediction using Eq. (11).

regime Φ_4 with the characteristic under-prediction for the remaining regimes. The under prediction of Eq. (11) is partially due to the manner by which the disk springs are constrained during testing. Eq. (11), as well as its predecessors, assumes that the displacement will not stop at the flat position, but will continue until the spring is fully inverted. This physical limitation creates the prominent stopper effect seen in all cases. Conversely, it can also be said that the theoretical load-deflection characteristics are, in essence, based on a single continuous nonlinear relationship [6] that is inherently dependent on the disk spring symmetry, and therefore, cannot be directly modified to account for the appearance of distinct regimes.

While good agreement between theoretical and measured load-displacement characteristics is apparent (Fig. 8), the hysteretic force difference — computed by subtracting unloading and loading curves of measured load-displacement characteristics — gives more insight at much finer resolution into what the hysteretic behavior is over each regime. The measured hysteretic force differences seen in configurations Υ_1, Υ_3, and Υ_4 (Figs. 9a, 9c, and 9d, respectively) are at similar levels, which lends credence to the assumption made when applying the determined value of μ_e from configuration Υ_1 to all other cases, which means that the disk springs and platen surfaces are relatively consistent between trials. The overall hysteresis characteristics of configurations Υ_1 and Υ_4 (Figs. 9a and 9d, respectively) are reasonably represented by the force difference of $P_F(\delta)$ with the determined coefficients of friction shown in Table 3. However, there is a pronounced linear behavior observed over regimes Φ_3 and Φ_4 in the measured characteristic of configurationΥ_3 shown in Fig. 9c (seen to a much lesser extent in configurations Υ_1 and Υ_4), which is not fully captured by prior or proposed models. As should be expected from the determination of μ_ϕ (Table 3), the hysteretic force difference in configuration Υ_2 is significantly higher

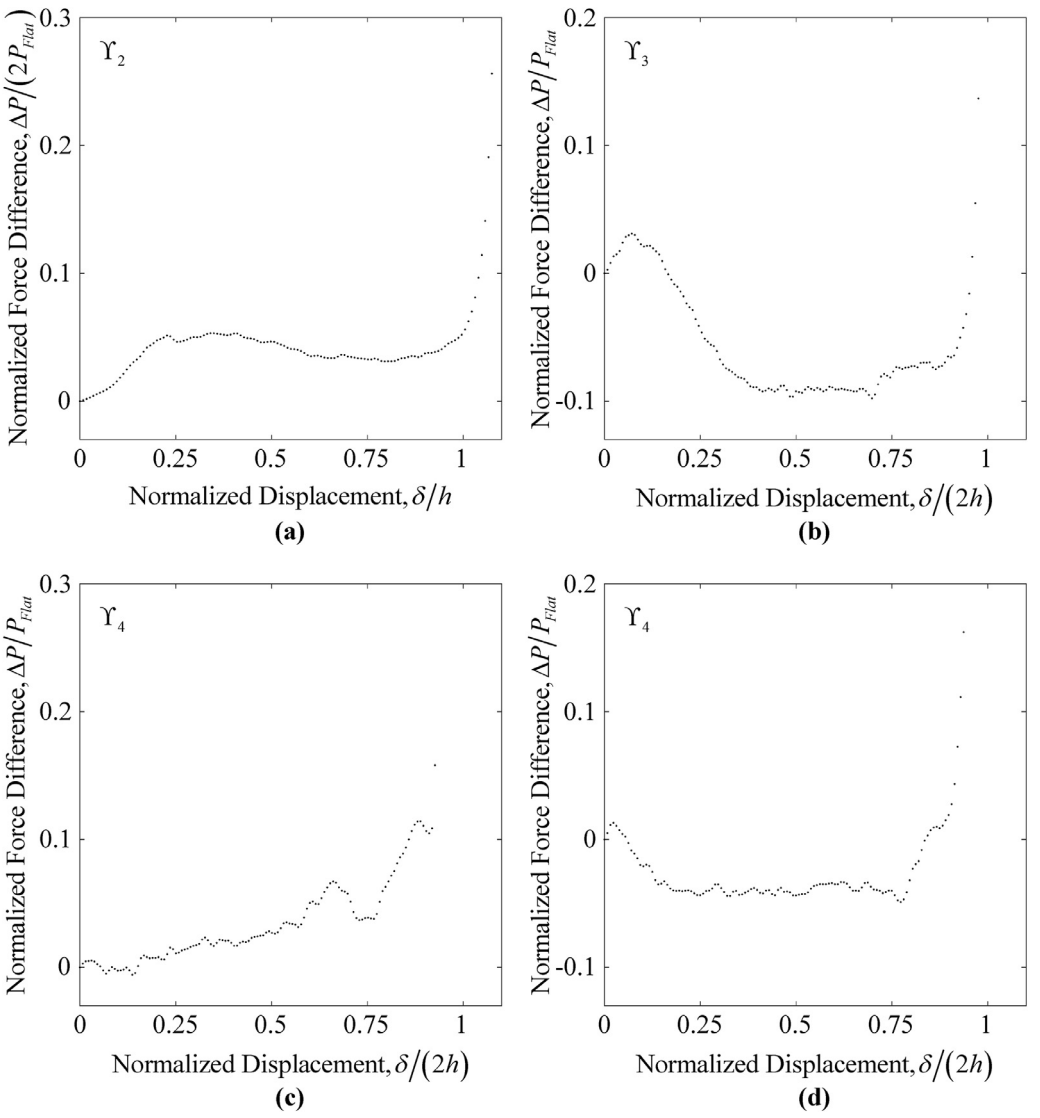

Fig. 10. Variations in measured hysteresis characteristics produced by disk spring pairings for three configurations of Table 1 and Fig. 2: (a) Υ_2, (b) Υ_3, (c) Υ_4 — variation of standard form (matched pair), (d) Υ_4 — variation produced with a poorly matched pair.

than any other configuration. Surprisingly, the hysteretic force difference (Fig. 9b) for the parallel stack (configuration Υ_2) is reasonably well predicted over displacement regimes Φ_2, Φ_3, and Φ_4 with theory deviating from measurement in the latter part of regime Φ_4.

The hysteresis characteristics of the atypical load-deflection measurements (Fig. 6) are computed in the same manner as described previously and the results are shown in Fig. 10. While significant differences between the load-deflection characteristics of the standard and variation of standard forms of configuration Υ_4 (Figs. 5d and 6c, respectively), deviations between these cases are minor when comparing their hysteretic force differences (Figs. 9d and 10c, respectively). Conversely, the atypical load-displacement forms of configurations Υ_3 and Υ_4 (Figs. 6b and 6d, respectively) yield a hysteresis force difference that has a negative force regime, shown in (Figs. 10b and 10d), which is due to the crossing of the loading and unloading characteristics for each of these configurations. The atypical load-deflection of configuration Υ_2 (Fig. 10a) shows a pronounced decrease in the hysteretic force from its typical counterpart (Fig. 9b), and is observed on all runs of spring pairs exhibiting these atypical load-deflection characteristics. In actuality, the hysteretic force difference of the atypical configuration Υ_2 (Fig. 10a) is closer to the hysteretic force values seen in the standard single disk spring case (configuration Υ_1 in Fig. 9a). This implies that there is hardly any relative motion between the parallel disk springs in these cases.

7. Nonlinear stiffness expression and comparisons with measurement

The displacement-dependent stiffness expression, as shown below, was presented by Almen and Laszlo [6] and was determined by differentiating Eq. (5) with respect to δ.

$$k_{L1}(\delta) = \frac{E\delta\pi\tau}{(1-\nu^2)a^2}\left(\frac{\alpha}{\alpha-1}\right)^2\left(\frac{\alpha+1}{\alpha-1}-\frac{2}{\ln\alpha}\right)\left(h^2-3\delta h+\frac{3\delta^2}{2}+t^3\right) \tag{13}$$

To the best of the author's knowledge, no further stiffness expressions have been presented in literature. Accordingly, a refined stiffness expression that is in agreement with the assumptions of this study is determined by differentiating Eq. (6) with respect to δ, and the result takes the following form.

$$k_{L2}(\delta) = \frac{E\delta\pi\tau}{a^2}\left(\frac{\alpha}{\alpha-1}\right)^2\left(\frac{\alpha+1}{\alpha-1}-\frac{2}{\ln\alpha}\right)\left(h^2-3\delta h+\frac{3\delta^2}{2}+t^3\right) \tag{14}$$

Minor differences between Eqs. (13) and (14) are due to slightly different load-defection relationships on which they are based. Eq. (14) describes displacement-dependent stiffness characteristics for each configuration of Table 1. Typical comparisons between theoretical and measured stiffness parameters (as computed from the measured load-deflection data) are displayed in Fig. 11 where the continuous nonlinearity is assumed over the entire displacement range. The poorest agreement between theoretical and measured stiffness, which is largely due to the increasing range of the stiffness characteristic, is observed with configurationΥ_2. As shown in Fig. 11b, theory represents only a limited range in regime Φ_3. This inaccuracy is redoubled since the range of accuracy in regime Φ_3 is in the middle; therefore, neither of the adjacent regimes is successfully predicted for configurationΥ_2 in Fig. 11b. The initial stiffening, regimes Φ_1 and Φ_2, arises from the incomplete contact between disk spring and platen for all configurations; this is also observed from the force perspective in Fig. 7. For configuration Υ_2, this effect is amplified because the gaps between parallel disk springs must be closed. To a much lesser extent, similar agreement is observed with configuration Υ_1 in Fig. 11a; however, a significant portion of regime Φ_3 is predicted acceptably, and the character of regime Φ_4 is preserved. Much closer agreement between theory and measurement is observed in the load-deflection curves, Fig. 7a, of configuration Υ_1. From the stiffness perspective, this added agreement observed with configuration Υ_1 between theoretical and measured stiffness may be attributed to the stiffness characteristics changing less quickly over relatively similar actual displacements. Likewise, much closer agreement between predicted and measured stiffness is observed in both of the series cases — Figs. 11c and 11d, respectively. It can be asserted that this is because configurations Υ_3 and Υ_4 possess close to double the displacement ranges of either configuration Υ_1 or Υ_2. It is of note that the load-deflection characteristics of configurations Υ_3 and Υ_4, Figs. 7c and 7d, have only acceptable agreement past regime Φ_3. However, it is important that the character of the load-deflection characteristic is preserved throughout most of regime Φ_4, which is directly responsible for the observed agreement between theory and measurement based stiffness parameters of configuration Υ_3 over regimes Φ_3 and Φ_4 (Fig. 11c). Considering the irregular nature of the load-deflection characteristic of configuration Υ_4 (Fig. 7d) compared to the other configurations, its stiffness characteristic (Fig. 11d) shows extraordinarily good agreement between theory and measurement over regimes Φ_3, Φ_4, and Φ_5. Nevertheless, a large disparity between theory and measurement is seen in regime Φ_6 in both value and character of the curve. This observed effect is due to the disparity in stiffness between the paired springs, and is clearly seen in Fig. 7d.

It is also of note that the theoretical predictions for all configurations cross the zero stiffness line and become negative, which implies that this particular disk spring should snap through in a buckling action. Almen and Laszlo [6] have shown that the disk spring in question should have a negative spring rate when the inequality $h > \tau\sqrt{2}$ is satisfied, as it is indeed done in this case. However, for configurations Υ_1, Υ_2, and Υ_3, the appearance of a negative stiffness regime does not occur. This divergence of experimental result from prediction is due to the physical constraint of the platen not allowing the disk spring to pass though the flat to the inverted displacement regime ($\delta > h - \tau$). Conversely, the stiffness of the configuration Υ_4 does cross zero, albeit to a much lesser extent in measurement than the prediction. The slight buckling action observed in the experimental configuration Υ_4 is a consequence of the mismatch between disk springs. It can also be asserted that if the disk springs of configuration Υ_4 were to be perfectly matched (in the sense of their respective load-displacement characteristics), the effects observed in Figs. 7d and 11d would be significantly lessoned.

8. Conclusion

The chief contribution of this article is the development of nonlinear load-deflection and nonlinear stiffness formulations for a single coned disk spring, the primary parallel stack configuration, and two primary series stack configurations. Specific contributions include the following. First, unlike the prior literature [2, 6, 17–21, 26], full-range load-deflection characteristics of a disk spring and primary stack configurations have been measured and analyzed to define nine naturally occurring transition points. A refined load-deflection formulation has been proposed to account for edge friction and interfacial friction between disk springs in configuration Υ_2 and is compared with prior theory [6, 17–20, 26]. The proposed formula is then employed to evaluate the values of μ_e and μ_ϕ from experimental results, as well as to assess the amount of hysteretic force. An updated continuously nonlinear displacement-dependent stiffness expression is then proposed and compared with measurements. However, the accuracy of continuous stiffness model is limited to only midrange displacement regimes as

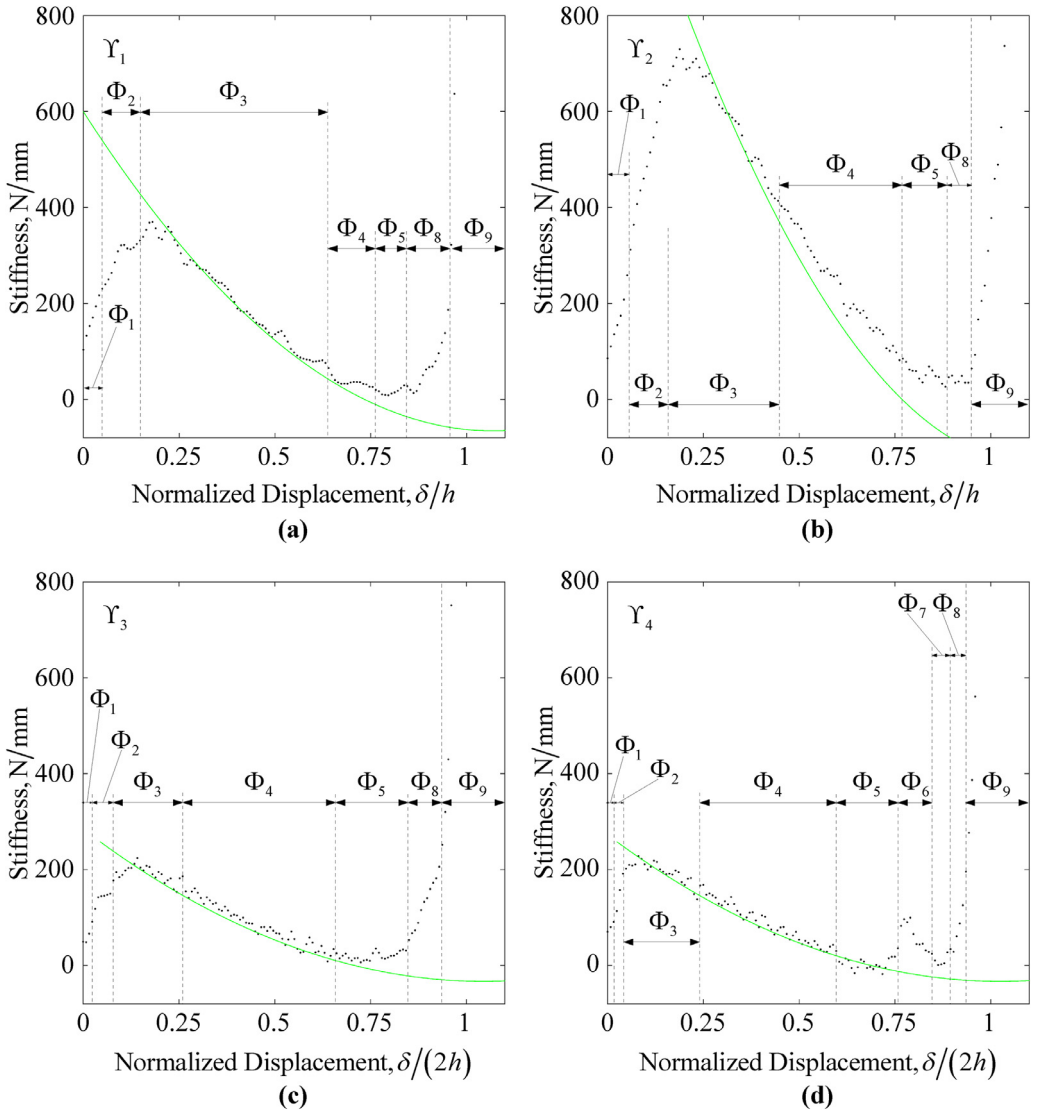

Fig. 11. Comparison between continuously nonlinear stiffness models with measurements for four configurations of Table 1 and Figs. 1 and 2: (a) Υ_1, (b) Υ_2, (c) Υ_3, and (d) Υ_4. Key: ●●●●● measurement, ▬ theoretical prediction using Eq. (14) by assuming continuous nonlinearity over the entire displacement range.

large deviations from the measurements at low and high displacements are found. Prior literature [15–26] has mostly ignored stiffness formulations as only one continuous formulation [6] has been discussed. This article enriches the coned disk literature [1–2, 4, 6, 15–26, 30], and the characterization methods contained herein should be applicable to diagram springs and other nonlinear devices over the specified displacement regime [12].

Some of the limitations of theory presented here are inherently limited by the assumptions employed by Almen–Laszlo [6] in the load-deflection relationship. These might be overcome if the disk spring formulation proposed by Hübner *et al.* [31–32] could be sufficiently modified to account for the appearance of distinct regimes since it is based on shell theory. Finally, dynamic experiments on mechanical systems with embedded the coned disks should be conducted to assess effective elastic and damping properties; such future studies should be valuable from the perspective of constructing quasi zero stiffness type isolators [7–13]

Acknowledgments

We acknowledge the Smart Vehicles Concepts Center (www.SmartVehicleCenter.org) and the National Science Foundation Industry/University Cooperative Research Centers program (www.nsf.gov/eng/iip/iucrc) for partially supporting this basic research.

References

[1] N.P. Chironis, New equations simplify Belleville spring design, Product Engineering (January) (1969) 116–118.
[2] P. Bühl, Maximale Höhen bei Tellerfedern aus Sonderwerkstoffen, DRAHT-Fachz. (2) (1974) 63–65.
[3] Schnorr Handbook for Disk Springs, 14th ed., Adolf Schnorr GmbH, Sindelfingen, Germany, 1983.
[4] C.K.H. Dharan, J.A. Bauman, Composite disc springs, Composites 38 (2007) 2511–2516.
[5] Precision Disc Springs, Century Spring Corp. and MW Industries Inc., Los Angeles, CA, and Baltimore, MD, USA 2015.
[6] J.O. Almen, A. Laszlo, The uniform-section disk spring, Trans. ASME 58 (1936) 305–313.
[7] A.M. Wahl, Initially coned disk (Belleville) springs, in: Mechanical Springs, 1st ed., Penton Publishing Company, Cleveland, OH, USA, 1944, pp. 238–262.
[8] G.J. Efstathiades, C.J.H. Williams, Vibration isolation using non-linear springs, Int. J. Mech. Sci. 9 (1967) 27–44.
[9] D. Muster, R. Plunkett, Isolation of vibrations, in: L.L. Beranek (Ed.), Noise and Vibration Control, Revised, ed. Institute of Noise Control Engineering, Washington D.C., USA, 1988, pp. 424–427.
[10] A. Carrella, M.J. Brennan, T.P. Waters, Optimization of a quasi-zero-stiffness isolator, J. Mech. Sci. Tech. 21 (2007) 946–949.
[11] C.-M. Lee, V.N. Goverdovskiy, A.I. Temnikov, Design of springs with “negative” stiffness to improve vehicle driver vibration isolation, J. Sound Vibration 302 (2007) 865–874.
[12] R.A. Ibrahim, Recent advances in nonlinear passive vibration isolators, J. Sound Vibration 314 (2008) 371–452.
[13] M. Schenk, S.D. Guest, On zero stiffness, Proc. IMechE Part C: J. Mech. Eng. Sci. 228 (10) (2013) 1701–1714.
[14] S. Timoshenko, Thin plates and shells, in: Strength of Materials Part II: Advanced Theory and Problems, 2nd ed., D. Van Nostrand Co., Inc., Lancaster, PA, USA, 1948, pp. 182–183.
[15] R. Schmidt, G.A. Wempner, The nonlinear conical spring, J. Appl. Mech. (December) (1959) 681–682.
[16] O. Lutz, Zur Berechnung der Tellerfedern, Konstruktion 12 (2) (1960) 57–59.
[17] G. Curti, M. Orlando, A new calculation of coned annular disk spring, in: Proceedings of ASME Winter Annual Meeting, New York, NY, USA, 1976 76-WA / DE-9.
[18] G. Curti, M. Orlando, Ein neues Berechnungsverfahren für Tellerfedern, DRAHT 30 (1) (1979) 17–22.
[19] G. Curti, M. Orlando, G. Podda, Vereinfachtes Verfahren zur Berechnung von Tellerfedern, DRAHT 31 (11) (1980) 789–792.
[20] G. Curti, R. Montanini, Theoretical, numerical, and experimental analysis of conical disk springs, in: XXV AIAS National Conference International Conference on Material Engineering, Gallipoli, Lecce, Italy, 1996, pp. 573–581.
[21] G. Curti, M. Orlando, G. Podda, Experimentelle Nachprüfung eines neuen Berechnungsverfahrens für Tellerfedern, DRAHT 31 (1) (1980) 26–29.
[22] D.H. Thiel, Friction in stacked-disk springs, in: Proceedings of ASME Winter Annual Meeting, Philadelphia, PA, USA, 1963 63-WA-270.
[23] K.-H. Muhr, P. Niepage, Über die Reduzierung der Reibung in Tellerfedersäulen, Konstruktion 20 (10) (1968) 414–417.
[24] P. Niepage, Über den Einfluß der Reibung und Kreiskegelförmiger Lasteinleitungselemente auf die Kennlinie von Einzeltellerfedern und Tellerfederpaketen, Konstruktion 36 (10) (1984) 379–384.
[25] G. Curti, R. Montanini, G. Barbato, Determinazione sperimentale del coefficiente di attrito in molle a disco conico, in: Atti IV Congr. Naz. Misure Mecc. E Termiche, Dipartimento di Energetica, Università degli Studi di L'Aquila, L'Aquila, Abruzzo, Italy, 1999, pp. 29–40.
[26] G. Curti, R. Montanini, On the influence of friction in the calculation of conical disk springs, Trans. ASME 121 (1999) 622–627.
[27] P. Bühl, Mechanische Schwingungen bei Tellerfedersäulen, DRAHT-Fachz. (2) (1977) 48–53.
[28] S. Ozaki, K. Tsuda, J. Tominaga, Analyses of static and dynamic behavior of coned disk springs: effects of friction boundaries, Thin-Walled Structures 59 (2012) 132–143.
[29] J.P. Den Hartog, Systems with variable or nonlinear characteristics, Mechanical Vibrations, 4th ed. New York, NY, USA: Dover Publications, Inc., 1985, ch. 8, sec. 8.8, pp. 370–373.
[30] N.P. Mastricola, J.T. Dreyer, R. Singh, Analytical and experimental characterization of nonlinear coned disk springs with focus on edge friction contribution to force-deflection hysteresis, Mech. Sys. Sig. Proc. 91 (2017) 215–232.
[31] W. Hübner, F.A. Emmerling, Axialsymmetrische große deformationen einer elastischen Kegelschale, ZAMM (62) (1982) 404–406.
[32] W. Hübner, Deformationen und Spannungen bei Tellerfedern, Konstruktion 34 (10) (1982) 387–392.